

Pion distributions in highly inelastic $pp \rightarrow p\pi X$ at 28.5 GeV/c and comparisons with $ep \rightarrow e\pi X^*$

E. W. Anderson,[†] T. S. Clifford, E. Lazarus,[‡] W. N. Schreiner, P. Schübelin,[§] and F. Turkot^{||}
Brookhaven National Laboratory, Upton, New York 11973

L. J. Gutay

Purdue University, West Lafayette, Indiana 47907

G. B. Collins, J. R. Ficenece, and B. C. Stringfellow^{||}

Virginia Polytechnic Institute and State University, Blacksburg, Virginia 24061

(Received 15 July 1975)

We have measured the π^- yield in $pp \rightarrow p\pi^- X$ relative to the cross section for $pp \rightarrow p + MM$ at 28.5 GeV/c. The pion distributions are parameterized in terms of x , p_{\perp}^2 , and ϕ in the rest frame of the missing mass, MM. The distributions are compared with the corresponding electroproduction case for $-0.1 < x < 0.6$ at the same missing mass and four-momentum transfer to the scattered beam particle. We find striking similarities: (1) The ϕ distributions are flat for the proton case as in electroproduction, (2) the slopes of the transverse-momentum distributions are the same as in electroproduction, and (3) the x distributions have the same shape as in electroproduction.

I. INTRODUCTION

The notion of comparing high-energy electron and proton scattering has existed now for approximately ten years. Wu and Yang¹ first suggested, and Abarbanel, Drell, and Gilman² further developed, the means by which high-energy elastic proton and electron data might be correlated. Berman and Jacob³ further extended these ideas to the inelastic case. By comparing 19-GeV/c proton scattering to deep-inelastic electroproduction, Allaby *et al.*,⁴ attempted, with mixed success, to find a relation between the electron structure function, W_2 , and a suitably defined proton analog.

Since the initial discovery by the SLAC-MIT collaboration⁵ of Bjorken scaling in $e+p \rightarrow e+MM$, a considerable effort has been expended in determining the final states which comprise the surprisingly large scaling cross section.⁶ Accompanying the large experimental program has been an equally exhaustive theoretical effort.⁷ As an extension of previous efforts to examine the relationship between electron and proton scattering, we report here a comparison of final states in

$$e+p \rightarrow e+MM, \quad (1)$$

$$p+p \rightarrow p+MM. \quad (2)$$

In particular, we study the pions comprising the missing mass MM:

$$e+p \rightarrow e+\pi+\text{anything}, \quad (3)$$

$$p+p \rightarrow p+\pi+\text{anything}. \quad (4)$$

II. KINEMATICS

In electroproduction the scattering proceeds through the exchange of a single virtual photon. Hence reaction (3) may be viewed as the simple inclusive reaction

$$\gamma_v + p \rightarrow \pi + \text{anything}, \quad (5)$$

where the virtual photon mass is just the four-momentum transfer,

$$q^2 = -(p_1 - p_3)^2, \quad (6)$$

and the total energy in the γ_v-p c.m. system is just the missing mass,

$$W = (p_1 + p_2 - p_3)^2, \quad (7)$$

where p_1 , p_2 , and p_3 are the four-momenta of the beam, target, and scattered particles, respectively. One may then determine $\gamma_v p$ cross sections for reaction (5) from the following factorization:

$$\frac{d\sigma}{dE'_e d\Omega_e dp_{\pi^3}} = \Gamma \frac{d\sigma}{dp_{\pi^3}}, \quad (8)$$

where the electron scatters into the solid angle $d\Omega_e$ with energy E'_e , Γ is the virtual photon flux, and $d\sigma/dp_{\pi^3}$ is the inclusive cross section for reaction (5). Combining Eq. (8) with the expression for the total $\gamma_v p$ cross section,

$$\frac{d\sigma}{dE'_e d\Omega_e} = \Gamma \sigma, \quad (9)$$

where σ is the total virtual photon-proton cross section, yields

$$\frac{E}{\sigma} \frac{d\sigma}{dp_{\pi^3}} = \frac{E}{d\sigma/dE'_e d\Omega_e} \frac{d\sigma}{dE'_e d\Omega_e dp_{\pi^3}}. \quad (10)$$

The expression on the right-hand side of Eq. (10) is simply the conditional probability (weighted by energy) of finding a pion in dp_π^3 given an electron in $dE'_e d\Omega_e$.

Because the proton scattering mechanism is not calculable, we shall compare the right-hand side of Eq. (10) with its counterpart for reaction (4) with a subscript e replaced by p .⁸ For notational convenience, though, and because of wide usage in the electron literature, we shall refer to both the electron and proton cross sections as

$$\frac{E}{\sigma} \frac{d\sigma}{dp^3}, \quad (11)$$

which should be strictly interpreted as the right-hand side of Eq. (10). We also refer to the four-momentum transfer to the scattered beam particle as a positive quantity,

$$t = (p_1 - p_3)^2 = -q^2 > 0. \quad (12)$$

III. THE MASS EXPERIMENT

The proton data presented here were obtained with the Multiparticle Argo Spectrometer System, MASS,⁹ at the Brookhaven National Laboratory AGS. The diffracted 28.5-GeV/ c proton beam was incident upon an 8-in. LH₂ target. The detector was triggered upon a fast forward proton in the high-momentum spectrometer of MASS. Momentum determination was provided by a pair of bending magnets with core readout chambers both before and after. Proton identification was accomplished with a CO₂ threshold Čerenkov counter. The charged particles comprising the missing mass were momentum-analyzed but not mass-identified in the vertex spectrometer (VS).¹⁰ The VS consisted of nine nested cylindrical magnetostrictive wire spark chambers surrounding the target with the cylinder axis normal to the laboratory floor. The chambers and target were immersed in a 10-kG magnetic field parallel to the cylinder axis.

Track losses in the VS due to sparking inefficiency were found to be negligible by three methods: (1) measurement of the efficiency for finding recoil particles in elastic events, (2) efficiency for finding those tracks detected by the external spectrometer, and (3) measurement of the sparking efficiency in reconstructed events. The sparking efficiency thus determined decreased from 98% for two-prong events to 95% for ten-prong events. The resulting track losses were well below 1%.

The track recognition code PITRACK¹¹ reconstructed the particle trajectories in the VS. The performance of the automatic track recognition was monitored by a manual scan of test samples of events by physicists. PITRACK was found to be 94% efficient in finding tracks, and only 1% of the

tracks found were spurious. The software inefficiency of 6% coupled with a 10% solid-angle loss and a 1% loss of particles due to the 80-MeV/ c range cutoff (for pions) yielded an over-all 17% inefficiency for detection of charged particles.

After track recognition, the tracks in an event were fitted by least squares to a common vertex. For the data presented here, the percentage of events failing the fit never exceeded 3.3% for any data point. Only those events passing the fit are presented in the following results. However, the absence of the events not successfully fitted does not affect the results presented.

In a certain fraction of the events accepted, no associated particles were found by PITRACK in the VS. An attempt was made to determine the effect of these one-prong events on the results. The percentage of these events in each data point is indicated in column 3 of Table I. It is evident that these one-prong events comprise a large segment of the data for low- t triggers. For the purpose of correcting multiplicities, samples of these events were manually scanned to determine to what extent

TABLE I. Fraction of events which are one-prong events and the factor for missing negative tracks for each data point.

W (GeV) (nominal)	$\langle t \rangle$ [(GeV/ c) ²]	Fraction of one-prong events	π^- weight
2.5	0.23	0.43	1.26
	1.01	0.11	1.13
3.5	0.23	0.46	1.21
	0.67	0.20	1.09
	0.99	0.09	1.08
	1.27	0.07	1.06
	1.84	0.05	1.04
4.5	0.43	0.38	1.12
	0.83	0.15	1.06
	1.11	0.07	1.05
	1.29	0.06	1.04
	1.49	0.05	1.03
	1.73	0.04	1.03
	2.12	0.03	1.02
	3.47	0.01	1.01
	3.98	0.02	1.01
4.79	0.01	1.005	
5.5	0.99	0.19	1.06
	1.41	0.06	1.03
	1.59	0.05	1.03
	2.11	0.03	1.02
	3.27	0.02	1.01
	3.61	0.01	1.006
	3.80	0.01	1.005
	4.00	0.01	1.005
4.23	0.01	1.005	
4.74	0.01	1.005	

PITRACK had failed to find legitimate tracks. On the basis of these scans, associated particle yields were corrected. Column 4 in Table I indicates the factor by which the number of negative tracks in each bin was corrected. Nevertheless, on the basis of the scanned sample, many of these one-prong events had no associated tracks. Because these one-prong events had only a single track at a small angle to the beam it is virtually impossible to determine on an event-by-event basis which ones originated in the target, as opposed to the chambers downstream of the target container. Rather, only an over-all statistical correction was made on the basis of target-empty runs. We can only note that the percentage of these events rises sharply at low t and with it the systematic uncertainty increases sharply.

The coordinate system is defined by the beam proton (z axis) and a normal to the scattering plane (y axis). The distributions of the event vertices along the three axes are shown for a sample of the data in Figs. 1 to 3. In the z distribution the peak near $z > 10$ cm reflects events originating in the vacuum chamber windows and the first spark chamber. The width of the x distribution is 50% larger than the beam because of resolution; however, the wider y distribution reflects the true beam size.

The kinematics of Eq. (2) at 28.5 GeV/c are illustrated in the Peyrou plot of Fig. 4, with contours of constant t and W indicated. The data were first divided into four missing-mass bands and then into t bins (minimum 1500 events/bin) to facilitate studying the process vs t . The data are generally divided into two sets: "low mass" data (40 000 events) at $W = 2.5$ and 3.5 GeV, for which $t < 2$ (GeV/c)², and "high mass" data (100 000

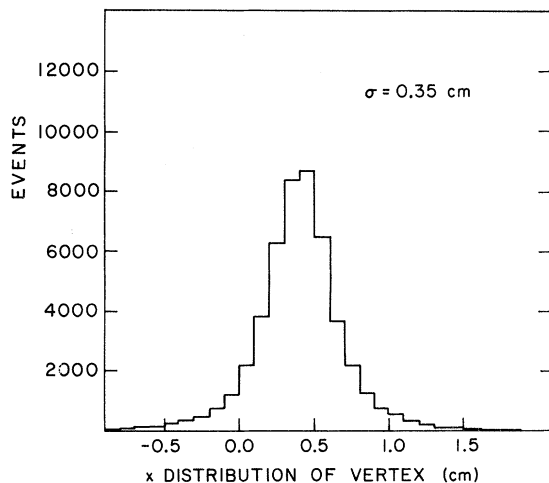


FIG. 1. Sample distribution of vertex x position for least-squares fitted events.

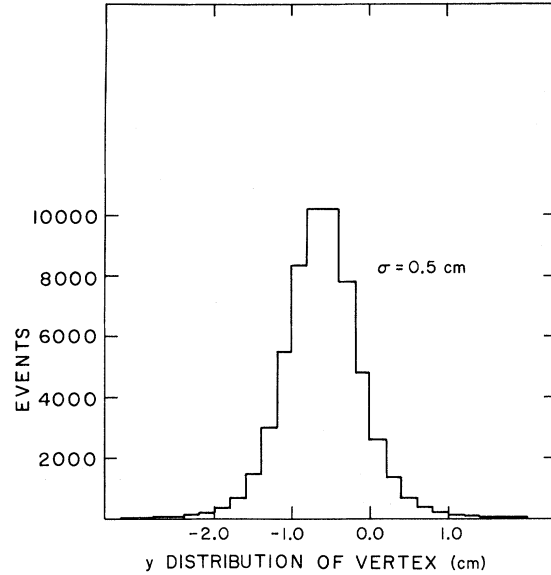


FIG. 2. Sample distribution of vertex y position for least-squares fitted events.

events) at $W = 4.5$ and 5.5 GeV, which extend to much higher momentum transfer, $t < 5$ (GeV/c)².

IV. RESULTS

Because there is no mass identification in the VS, we present pion distributions only for negative tracks and make the usual assumption that they are pions. As in electroproduction, we transform these pions to the rest frame of the missing mass and evaluate $(E/\sigma)(d\sigma/dp^3)$. In the new coordinate system, as is conventional, the z axis is in the direction of the missing mass and the y axis is normal to the proton scattering plane. In the missing-mass rest frame the cross section is evaluated in terms of $x = p_L/p_{\max}$, p_{\perp}^2 , and ϕ .¹²

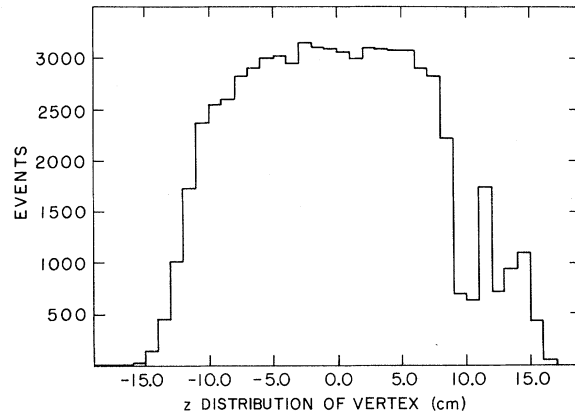


FIG. 3. Sample distribution of vertex z position for least-squares fitted events.

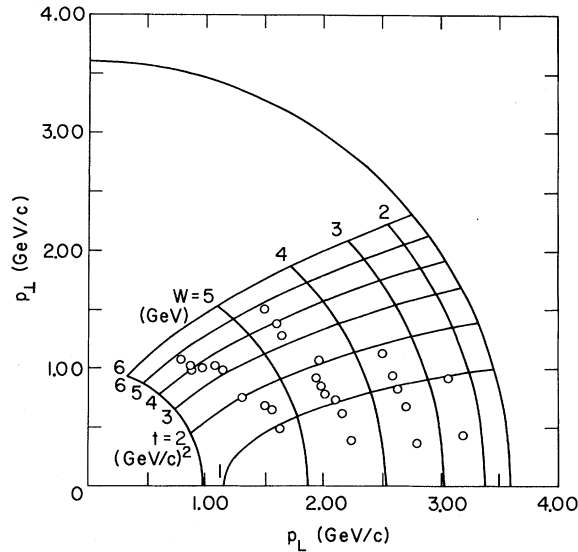


FIG. 4. Peyrou plot for $pp \rightarrow pX$ at 28.5 GeV/c with contours of constant t and W . Circles represent centers of bins used in this analysis.

A. Associated charge multiplicity

In Fig. 5, the associated charge multiplicities for Eqs. (1) and (2) are compared as a function of t at two values of missing mass. For $t < 2$ (GeV/c)², there is general agreement between lepton¹³⁻¹⁵ and proton results.¹⁶ At higher t , where only Cornell data are available, the proton multiplicity rises whereas the electron multiplicity is flat or slightly decreasing. In the electron data only the average charged multiplicity is available for $t > 2$ (GeV/c)²; hence we will not be able to compare pion momentum distributions in the region of large t where a difference in multiplicities is seen.

B. Pion distributions

Because of aperture losses at $x < 0$ and poor momentum resolution for large positive x , the pion distributions presented from the proton data have been restricted to $-0.1 < x < 0.6$. This restriction eliminates the need for detailed Monte Carlo calculations and folding of resolution functions. Hence our comparison is limited to central x or what is referred to in electroproduction as the virtual photon fragmentation region.

1. Distributions in ϕ

The ϕ distribution of π^- ,

$$\int \frac{2E}{\sigma p_{\max}} \frac{d\sigma}{dx dp_{\perp}^2 d\phi} dp_{\perp}^2,$$

is shown in Fig. 6 for two sample data points of the proton data in $0.0 < x < 0.2$.¹⁷ The plots, which

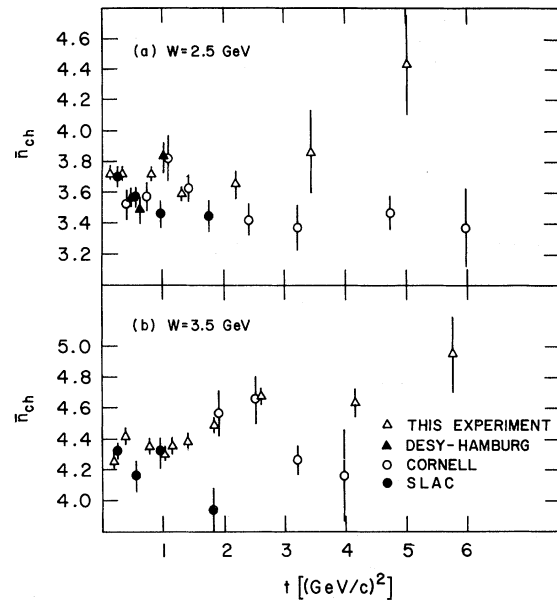


FIG. 5. Comparison of total charged-particle multiplicity in $pp \rightarrow pX$ and $ep \rightarrow eX$ as a function of t for (a) $W = 2.5$ GeV and (b) $W = 3.5$ GeV.

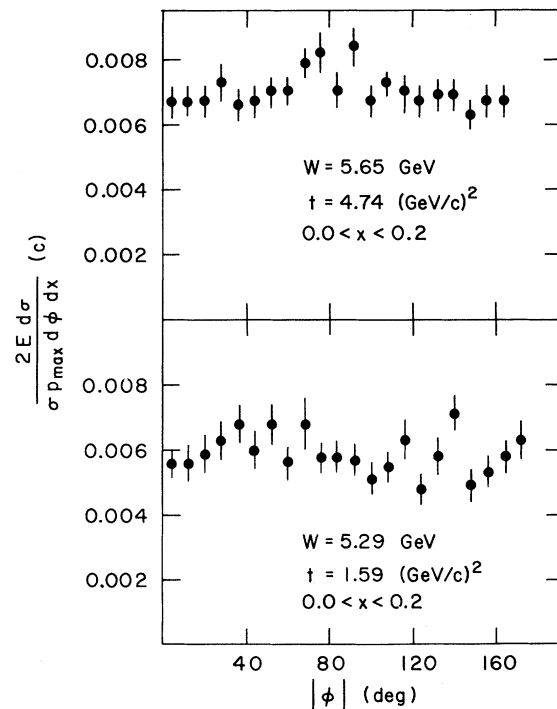


FIG. 6. Examples of the azimuthal angle distribution, $(2E/\sigma p_{\max})d\sigma/d\phi dx$ for $0.0 < x < 0.2$. Note that the distribution has been folded at $\phi = 0$ by plotting $|\phi|$.

are representative of all of the data in $-0.1 < x < 0.6$, are consistent with an isotropic distribution. In electroproduction, the ϕ distribution may be of the form

$$A + B \cos(\phi) + C \cos(2\phi).$$

Many electron experiments have searched for anisotropy^{14, 18-20}; however, it has not been observed to any significant degree except for $x \approx 0.7$.

2. p_{\perp}^2 distributions

The transverse-momentum distributions, averaged over ϕ for several cuts in x , have been fitted to the form

$$\frac{E}{\pi p_{\max} \sigma} \frac{d\sigma}{dx dp_{\perp}^2} = A e^{-B p_{\perp}^2}$$

over the range $0.04 < p_{\perp}^2 < 0.5$ (GeV/c)². An example of a transverse-momentum distribution is shown in Fig. 7 for $W = 4.48$ GeV and $t = 0.82$ (GeV/c)². The results for all of the proton data are displayed in Table II. They are shown graphically

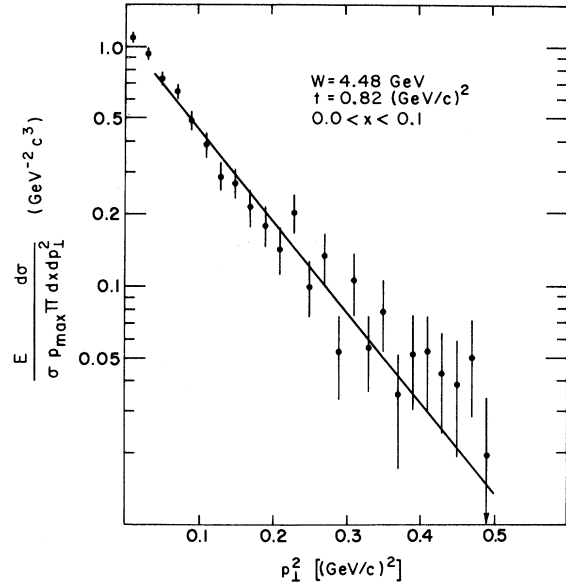


FIG. 7. Example of π^- transverse-momentum distribution in $pp \rightarrow p\pi^- X$ for $W = 4.48$ GeV and $t = 0.82$ (GeV/c)².

TABLE II. Fitted parameters of $(E/\sigma)d\sigma/dp^3 = A e^{-B p_{\perp}^2}$ for different x regions.

W (GeV)	t [(GeV/c) ²]	-0.1 < x < 0.0		0.0 < x < 0.1		0.1 < x < 0.2		0.2 < x < 0.4	
		A (GeV ⁻² c ³)	B [(GeV/c) ⁻²]	A (GeV ⁻² c ³)	B [(GeV/c) ⁻²]	A (GeV ⁻² c ³)	B [(GeV/c) ⁻²]	A (GeV ⁻² c ³)	B [(GeV/c) ⁻²]
2.54	0.23	0.48±0.08	8.0±0.8	0.52±0.09	9.4±0.9	0.59±0.09	8.0±0.7	0.39±0.05	7.0±0.5
2.58	1.01	0.90±0.11	10.8±1.0	0.83±0.10	8.0±0.9	0.84±0.10	8.5±0.9	0.54±0.05	6.7±0.5
3.48	0.23	0.51±0.07	6.9±0.6	0.72±0.08	8.4±0.5	0.48±0.07	6.9±0.6	0.35±0.04	6.1±0.4
3.54	0.67	0.73±0.08	8.2±0.6	1.07±0.09	8.7±0.5	0.65±0.07	6.8±0.6	0.57±0.06	7.9±0.5
3.59	0.99	0.93±0.08	8.9±0.6	1.09±0.09	8.9±0.6	0.87±0.09	7.7±0.7	0.65±0.06	7.5±0.6
3.60	1.27	0.70±0.07	7.6±0.7	1.11±0.09	9.0±0.6	0.94±0.09	8.2±0.6	0.46±0.04	5.4±0.4
3.61	1.84	0.79±0.09	6.9±0.8	1.01±0.12	8.6±0.8	0.90±0.13	8.0±1.1	0.46±0.05	5.6±0.6
4.44	0.43	0.58±0.06	7.1±0.5	0.73±0.07	7.3±0.4	0.62±0.07	7.0±0.5	0.34±0.04	5.7±0.4
4.47	0.83	0.78±0.06	7.7±0.4	1.09±0.08	8.8±0.4	0.87±0.07	7.8±0.5	0.44±0.04	5.8±0.4
4.50	1.11	0.89±0.05	7.7±0.3	1.07±0.06	8.1±0.3	0.82±0.05	7.0±0.4	0.60±0.04	6.8±0.3
4.60	1.29	0.98±0.05	8.4±0.4	1.20±0.06	8.8±0.4	0.96±0.06	7.2±0.4	0.46±0.03	5.5±0.3
4.61	1.49	0.86±0.06	7.7±0.5	1.13±0.07	8.0±0.4	1.01±0.07	7.9±0.4	0.53±0.04	6.5±0.4
4.62	1.73	0.94±0.07	7.7±0.5	1.15±0.08	8.4±0.4	1.07±0.09	8.6±0.5	0.50±0.04	6.2±0.5
4.49	2.12	1.06±0.11	9.3±0.8	1.17±0.10	8.6±0.6	1.11±0.12	8.6±0.8	0.56±0.07	7.1±0.8
4.71	3.47	1.28±0.12	8.4±0.7	1.52±0.13	8.6±0.6	0.82±0.10	7.1±0.8	0.38±0.05	5.7±0.6
4.67	3.98	1.21±0.10	7.8±0.6	1.76±0.15	9.6±0.6	0.95±0.10	7.1±0.6	0.34±0.04	4.3±0.6
4.65	4.79	1.11±0.12	7.4±0.8	1.61±0.17	9.2±0.8	1.06±0.13	6.8±0.8	0.29±0.04	4.8±0.7
5.22	0.99	0.85±0.06	7.9±0.4	0.96±0.06	7.5±0.4	0.70±0.06	6.5±0.4	0.40±0.03	5.3±0.4
5.24	1.41	1.05±0.06	8.6±0.4	1.28±0.07	8.1±0.3	0.93±0.07	7.4±0.5	0.47±0.03	6.0±0.4
5.29	1.59	1.10±0.07	8.6±0.4	1.25±0.07	8.0±0.4	0.97±0.08	7.6±0.5	0.50±0.04	6.0±0.4
5.46	2.11	1.00±0.07	7.8±0.5	1.36±0.08	8.0±0.4	0.92±0.07	6.5±0.4	0.45±0.04	5.9±0.4
5.45	3.27	1.17±0.07	7.4±0.4	1.50±0.09	7.9±0.4	0.90±0.07	6.3±0.4	0.37±0.04	5.9±0.5
5.48	3.61	1.19±0.06	7.3±0.3	1.53±0.08	8.1±0.4	0.91±0.06	6.4±0.4	0.26±0.02	4.2±0.4
5.58	3.80	1.34±0.06	7.9±0.3	1.57±0.07	7.5±0.3	0.88±0.05	6.5±0.3	0.29±0.02	5.0±0.4
5.66	4.00	1.30±0.06	7.8±0.3	1.63±0.07	7.8±0.3	0.91±0.05	6.5±0.3	0.26±0.02	4.3±0.4
5.63	4.23	1.34±0.06	7.5±0.3	1.63±0.07	8.0±0.3	1.04±0.06	7.2±0.3	0.26±0.02	4.6±0.4
5.65	4.74	1.38±0.06	7.8±0.3	1.54±0.06	7.3±0.2	0.85±0.05	6.1±0.3	0.26±0.02	4.8±0.4

for several values of x for $W=4.5$ and 5.5 GeV in Figs. 8–10. There is no significant change in slope parameter B throughout the entire range of t . The amplitude parameter A rises with increasing t and exhibits a flattening for $t > 3.0$ (GeV/c)². For $t < 1.0$ (GeV/c)² the rise is due entirely to the presence of the one-prong events, whose difficulty of interpretation has been emphasized. However, the behavior for $t > 1$ (GeV/c)² is unaffected by systematic corrections. In contrast, the slope parameter is independent of t over the entire range. Hence the ratio A/B , which is proportional to the partial multiplicity in a slice of x , increases with t . Indeed, for $W=4.5$ and 5.5 GeV dramatic increases in associated multiplicity have been observed in these data.¹⁶

In Fig. 11 we compare the transverse-momentum slope with the results from a SLAC electron experiment.²⁰ The t dependence of the slope parameter is compared in Fig. 11(a) for fixed W and x . Both data sets indicate independence of t at approximately the same value of B . In Fig. 11(b), B is compared as a function of x for fixed t and W . Again the agreement is quite good in the overlapping region of x . At $W=2.5$ GeV we compare both A and B parameters near $x=0$ with results from Cornell and DESY^{14, 21, 22}; see Fig. 12. The comparison with the Cornell data is clouded by their use of π^+ in the final state. Because the π^+ -to- π^- ratio in electroproduction is greater than one, a direct comparison of the A parameter is not possible. However, there is general agreement of both A and B for both sets of electroproduction data.

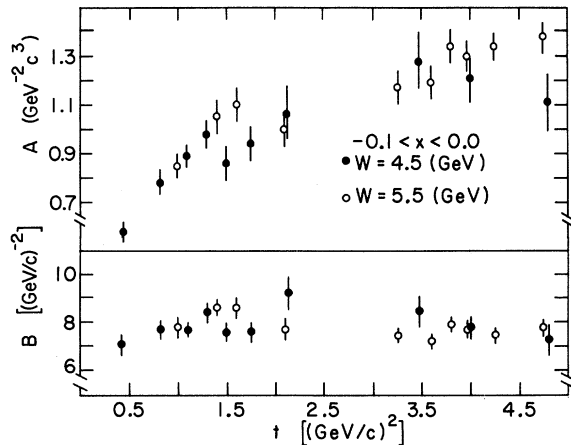


FIG. 8. Results of fit to transverse-momentum distribution $(E/\sigma)d\sigma/dp^3 = Ae^{-Bp_{\perp}^2}$ for $-0.1 < x < 0.0$ in $pp \rightarrow p\pi^-X$. The t dependence of the parameters is shown for $W=4.5$ GeV and $W=5.5$ GeV.

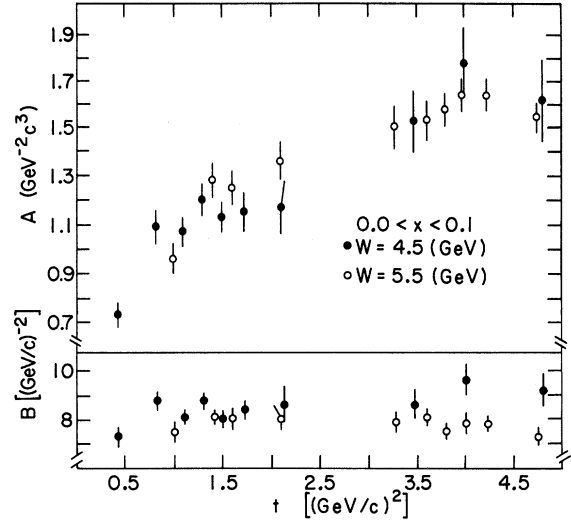


FIG. 9. Results of fit to transverse-momentum distribution $(E/\sigma)d\sigma/dp^3 = Ae^{-Bp_{\perp}^2}$ for $0.0 < x < 0.1$ in $pp \rightarrow p\pi^-X$. The t dependence of the parameters is shown for $W=4.5$ GeV and $W=5.5$ GeV.

3. x distributions

We have fitted both the x distributions integrated over p_{\perp}^2

$$F(x) = \int \frac{E}{\pi p_{\max} \sigma} \frac{d\sigma}{dx dp_{\perp}^2} dp_{\perp}^2 = A' e^{-B'x}$$

and the x distribution for small p_{\perp}^2

$$\frac{E}{\pi p_{\max} \sigma} \frac{d\sigma}{dx dp_{\perp}^2} = A'' e^{-B''x}$$

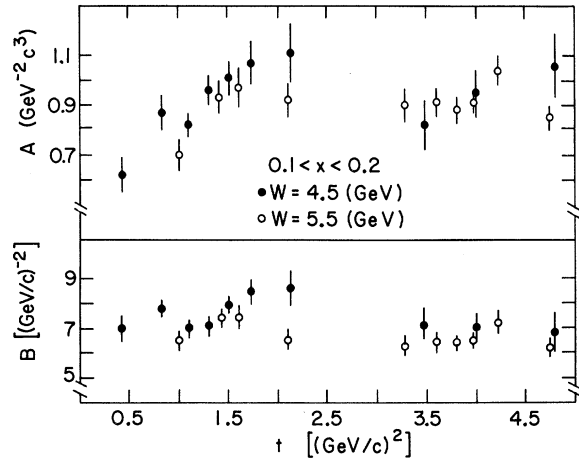


FIG. 10. Results of fit to transverse-momentum distribution $(E/\sigma)d\sigma/dp^3 = Ae^{-Bp_{\perp}^2}$ for $0.1 < x < 0.2$ in $pp \rightarrow p\pi^-X$. The t dependence of the parameters is shown for $W=4.5$ GeV and $W=5.5$ GeV.

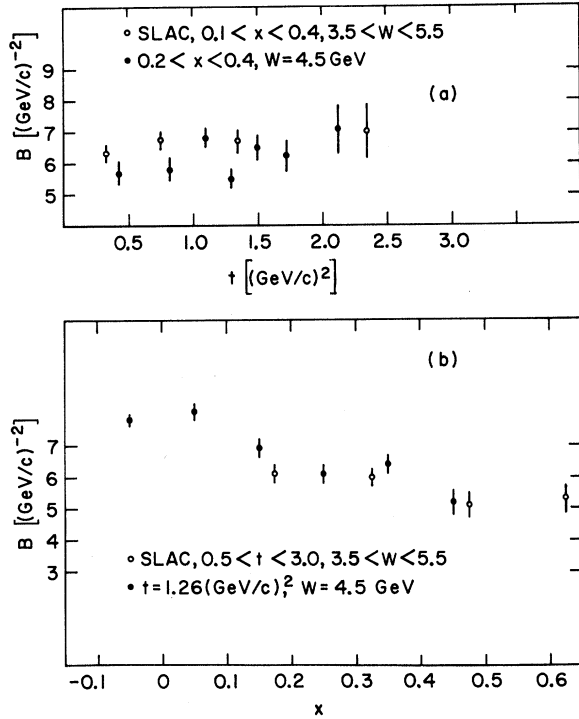


FIG. 11. A comparison of the slope parameters for the transverse-momentum distribution $(E/\sigma)d\sigma/dp^3 = Ae^{-Bp^2}$ with electroproduction results: (a) as a function of t , (b) as a function of x . The open circles are from Ref. 20.

over the range $0.08 < x < 0.6$. As mentioned above, the x distribution outside this range suffers from systematic uncertainties. However, as an example, Fig. 13 demonstrates that the shape of the full x distribution is remarkably similar to that seen in electroproduction. The full x distributions for all t and W intervals investigated here have the same general features, namely, they are rounded near zero and have a steeper slope for $x < 0$ than for $x > 0$.

The results for the fits in the range $0.08 < x < 0.6$ are shown in Table III. Examples of fits to $F(x)$ are shown in Fig. 14 for nominally fixed W and three values of t . Even without a fit it is clear from this figure that the higher t has a steeper slope. In Fig. 15 the B' parameters for fits to $F(x)$ are plotted for all t and W bins. Two distinct regions are seen: (1) For $t > 2.5 (\text{GeV}/c)^2$, B' is almost independent of t , and (2) for $t < 2.5 (\text{GeV}/c)^2$, it rises monotonically. The A' parameters for the fits to $F(x)$ are shown in Fig. 16. The interpretation here is less clear owing to the systematic uncertainties for small t . Nevertheless, for $1.0 < t < 2.5 (\text{GeV}/c)^2$, A' is rising slowly, while for $t > 2.5 (\text{GeV}/c)^2$, the increase in A' is much more dramatic. The results of the fits to

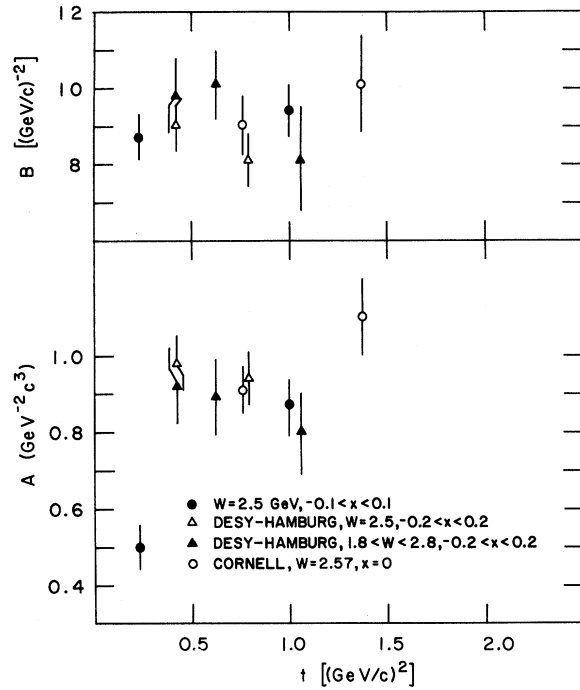


FIG. 12. Comparison of fitted parameters for $(E/\sigma) \times d\sigma/dp^3 = Ae^{-Bp^2}$ with electroproduction results at $W = 2.5 \text{ GeV}$.

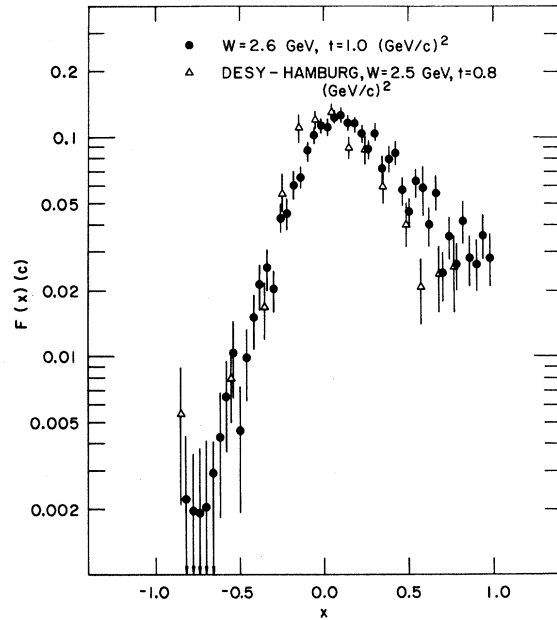


FIG. 13. A comparison of $F(x)$ with electroproduction for $t = 1 (\text{GeV}/c)^2$ and $W = 2.5 \text{ GeV}$. Systematic uncertainties in the proton data outside of $-0.1 < x < 0.6$ are known to be significant.

TABLE III. Fitted parameters for $(E/\sigma)d\sigma/dp^3 = A''e^{-B''x}$ with $p_{\perp}^2 < 0.04$ (GeV/c)² and for $F(x) = A'e^{-B'x}$.

W (GeV)	t [(GeV/c) ²]	$F(x) = A'e^{-B'x}$		$\frac{E}{\sigma} \frac{d\sigma}{dp^3} = A''e^{-B''x}$ $p_{\perp}^2 < 0.04$ (GeV/c) ²	
		A' (c)	B'	A'' (GeV ⁻² c ³)	B''
2.54	0.23	0.108 ± 0.008	1.9 ± 0.2	0.82 ± 0.10	2.8 ± 0.3
2.58	1.01	0.157 ± 0.008	2.0 ± 0.2	1.28 ± 0.12	3.6 ± 0.4
3.48	0.23	0.120 ± 0.010	2.3 ± 0.2	0.86 ± 0.11	3.5 ± 0.4
3.54	0.67	0.166 ± 0.010	2.5 ± 0.2	1.13 ± 0.12	3.5 ± 0.4
3.59	0.99	0.175 ± 0.009	2.1 ± 0.2	1.35 ± 0.12	3.1 ± 0.4
3.60	1.27	0.177 ± 0.009	2.2 ± 0.2	1.34 ± 0.11	3.4 ± 0.4
3.61	1.84	0.184 ± 0.012	2.4 ± 0.3	1.73 ± 0.22	4.7 ± 0.6
4.44	0.43	0.150 ± 0.010	3.1 ± 0.2	1.13 ± 0.15	5.7 ± 0.5
4.47	0.83	0.178 ± 0.009	2.6 ± 0.2	1.42 ± 0.13	4.6 ± 0.4
4.50	1.11	0.209 ± 0.007	2.8 ± 0.1	1.52 ± 0.10	4.0 ± 0.3
4.60	1.29	0.212 ± 0.008	2.8 ± 0.1	1.57 ± 0.11	4.3 ± 0.3
4.61	1.49	0.214 ± 0.009	2.8 ± 0.2	1.41 ± 0.11	3.4 ± 0.3
4.62	1.73	0.219 ± 0.010	3.0 ± 0.2	1.53 ± 0.13	4.3 ± 0.4
4.49	2.12	0.209 ± 0.013	2.8 ± 0.3	1.68 ± 0.18	4.8 ± 0.5
4.71	3.47	0.255 ± 0.019	3.6 ± 0.3	1.89 ± 0.26	5.6 ± 0.7
4.67	3.98	0.282 ± 0.018	3.9 ± 0.3	1.80 ± 0.23	5.1 ± 0.7
4.65	4.79	0.338 ± 0.024	4.8 ± 0.3	1.75 ± 0.27	5.6 ± 0.8
5.22	0.99	0.203 ± 0.010	3.4 ± 0.2	1.71 ± 0.18	6.6 ± 0.5
5.24	1.41	0.242 ± 0.010	3.6 ± 0.2	1.94 ± 0.19	6.2 ± 0.5
5.29	1.59	0.254 ± 0.011	3.6 ± 0.2	2.10 ± 0.19	6.4 ± 0.5
5.46	2.11	0.255 ± 0.012	3.6 ± 0.2	1.74 ± 0.20	6.5 ± 0.6
5.45	3.27	0.320 ± 0.016	4.8 ± 0.2	2.16 ± 0.26	7.4 ± 0.7
5.48	3.61	0.335 ± 0.015	5.1 ± 0.2	1.94 ± 0.18	6.5 ± 0.5
5.58	3.80	0.336 ± 0.014	5.3 ± 0.2	2.35 ± 0.20	7.7 ± 0.5
5.66	4.00	0.349 ± 0.014	5.5 ± 0.2	2.61 ± 0.23	8.4 ± 0.5
5.63	4.23	0.356 ± 0.014	5.7 ± 0.2	2.49 ± 0.23	8.6 ± 0.6
5.65	4.74	0.361 ± 0.014	5.8 ± 0.2	2.70 ± 0.23	8.9 ± 0.5

the x distribution at small p_{\perp}^2 are shown in Figs. 17 and 18. Since the data in these fits are a subset of the $F(x)$ data, the percentage errors are about twice as large. Both parameters exhibit the same general behavior of increasing with t , but different rates of rise below and above $t = 2.5$ (GeV/c)² are difficult to discern.

In Fig. 19, proton data at $W = 2.5$ are compared with DESY streamer-chamber data.¹⁴ The agreement is reasonable; however, the electron data fall faster in x than do the proton data. In Fig. 20, higher-mass proton data are compared with SLAC electron data²⁰ for (a) $t = 0.43$ (GeV/c)², (b) $t = 0.83$ (GeV/c)², (c) $t = 1.49$ (GeV/c)², and (d) $t = 2.12$ (GeV/c)². In contrast to the previous comparison the electroproduction data are systematically higher than the proton data, the difference

becoming smaller with increasing t . Some of this difference is due to π^- from ρ decay which populate this region of x , and this becomes relatively less important with increasing t . The slopes of these distributions, however, are approximately the same. In Fig. 21, we compare $(E/\pi p_{\max} \sigma)(d\sigma/dx dp_{\perp}^2)$ with Cornell-Harvard electroproduction data¹⁹ on π^- at $W = 2.5$ GeV. The agreement in both slope and amplitude is quite good.

V. SUMMARY AND CONCLUSIONS

Our comparison of electron and proton scattering has led us to conclude the following for $t < 2.5$ (GeV/c)², $2.0 < W < 4.0$ GeV, and $-0.1 < x < 0.6$:

- (1) The average number of charged tracks is the same.

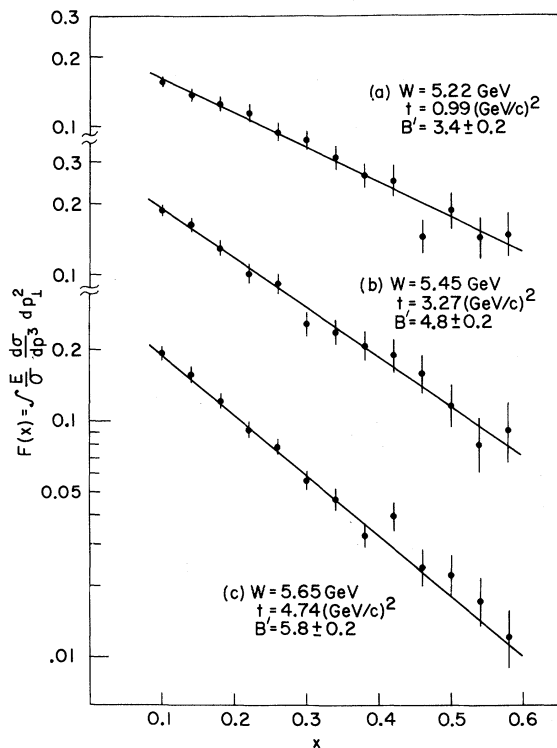


FIG. 14. The longitudinal distribution $F(x)$ with missing mass nominally constant at $W = 5.5 \text{ GeV}$ for (a) $t = 0.99 (\text{GeV}/c)^2$, (b) $t = 3.27 (\text{GeV}/c)^2$, and (c) $t = 4.74 (\text{GeV}/c)^2$. The variation of the slope parameter B with t is evident.

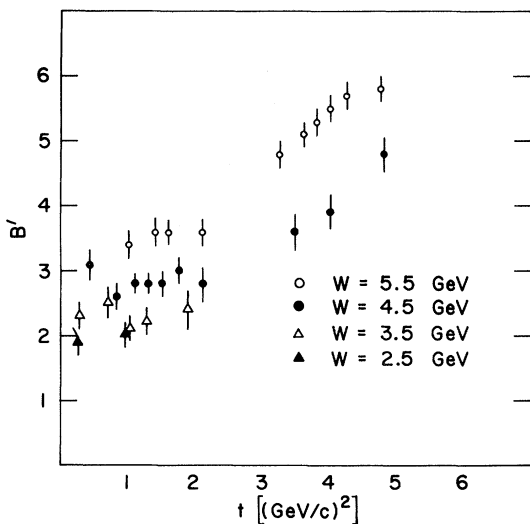


FIG. 15. Fitted slope parameter of the invariant cross section $F(x) = A'e^{-B'x}$ for $0.08 < x < 0.6$ as a function of t for various missing mass intervals.

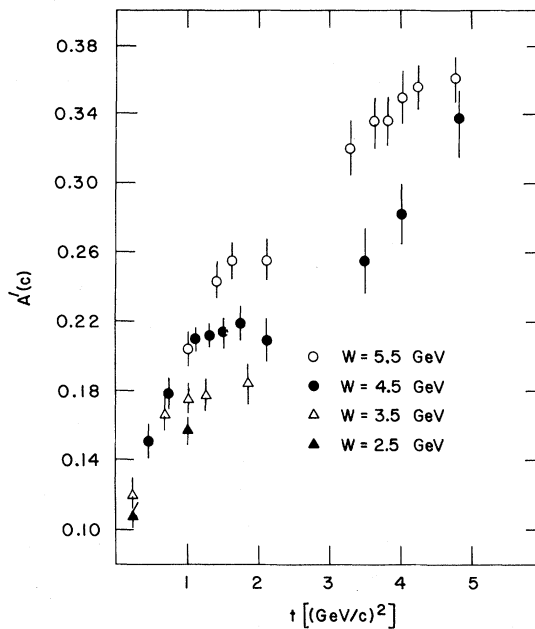


FIG. 16. Fitted amplitude parameter of the invariant cross section $F(x) = A'e^{-B'x}$ for $0.08 < x < 0.6$ as a function of t for various missing mass intervals.

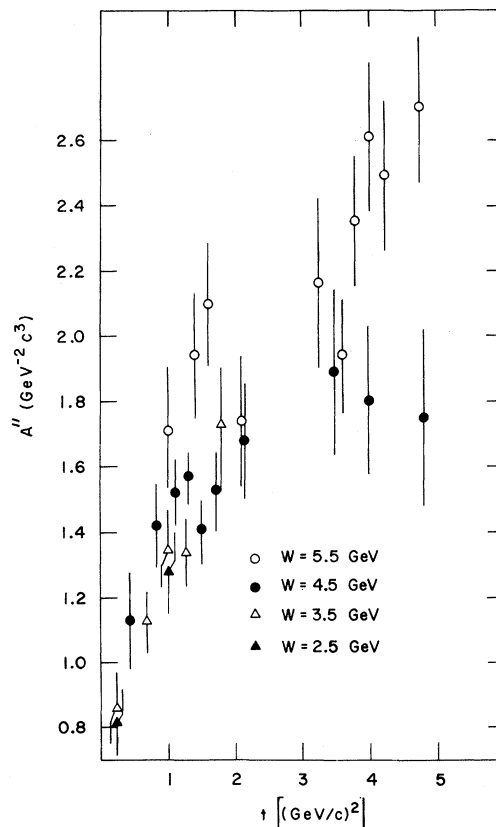


FIG. 17. Fitted amplitude parameter of the invariant cross section $(E/\sigma)d\sigma/dp^3 = A''e^{-B''x}$ for $p_{\perp}^2 < 0.04 (\text{GeV}/c)^2$ as a function of t for various missing mass intervals.

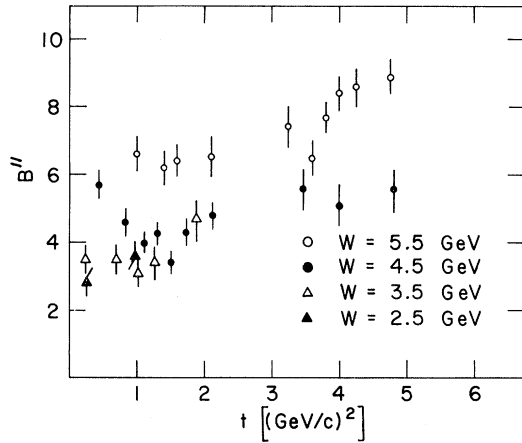


FIG. 18. Fitted slope parameter of the invariant cross section $(E/\sigma)d\sigma/dp^3 = A''e^{-B''x}$ for $p_{\perp}^2 < 0.04$ $(\text{GeV}/c)^2$ as a function of t for various missing mass intervals.

(2) The pion distribution in ϕ for both cases is flat.

(3) The transverse-momentum distributions of pions have the same slope and approximately the same amplitude.

(4) The pion distributions in x fall at approximately the same rate although a difference in amplitude is seen in some of the data.

The similarity between ep and pp inelastic collisions noted in statements (2)–(4) above is quite remarkable and unexpected. That \bar{n}_c is the same for the same W (at low t) is not too surprising in view

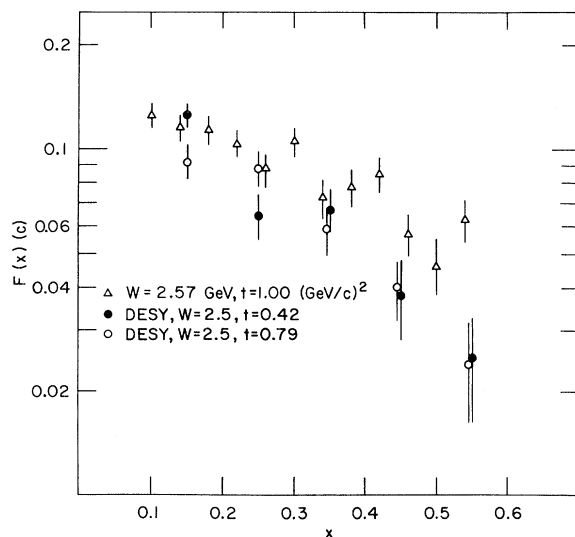


FIG. 19. Comparison of the invariant cross section $F(x)$ with DESY-Hamburg electroproduction results for $W = 2.5$ GeV.

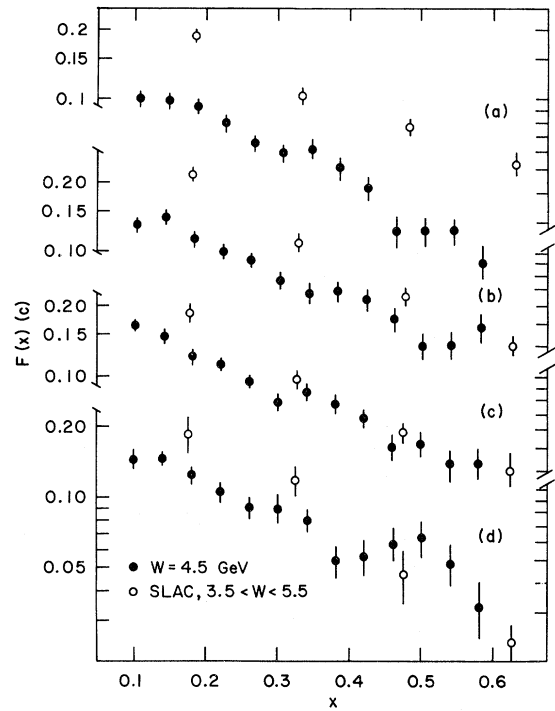


FIG. 20. Comparison of the invariant cross section $F(x)$ with SLAC electroproduction results for (a) $t = 0.43$ $(\text{GeV}/c)^2$, (b) $t = 0.83$ $(\text{GeV}/c)^2$, (c) $t = 1.49$ $(\text{GeV}/c)^2$, and (d) $t = 2.12$ $(\text{GeV}/c)^2$.

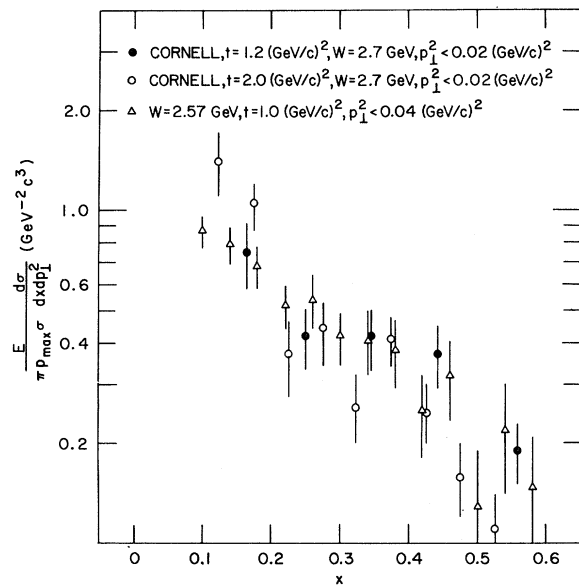


FIG. 21. Comparison of the invariant cross section $(E/d)d\sigma/dp^3$ with Harvard-Cornell electroproduction results for small p_{\perp}^2 and $W = 2.5$ GeV.

of the ubiquitous relationship found experimentally between \bar{n}_c and W .²³ However, the likeness in the detailed π^- distributions is surprising. Current theoretical descriptions regard the deep-inelastic ep electromagnetic scattering process as a pointlike virtual photon interacting with pointlike charged constituents in the target proton. These constituents, however, are not ejected from the target; rather, the four-momentum transmitted to them appears in the final state distributed among more familiar hadrons. On the other hand, since protons are not pointlike, it is difficult to imagine that a beam proton probes a target proton in a pointlike fashion via the strong interaction. Indeed, the probability that a target proton scatters an incident electron into a given t and W region is quite different from the probability that it scatters an incident proton into the same region (e.g., $ep/pp \sim 10^{-3}$ at $W=4$, $t=3$). Furthermore, there is no obvious Bjorken scaling in deep-inelastic pp scattering. Yet the response of the target proton in the two cases (at least in the common region surveyed here) is strikingly similar. It is as if the target system goes through the same intermediate state in both reactions prior to pion emission. One way

such an intermediate state could arise is if the constituents are so strongly bound in the target proton that, regardless of whether the four-momentum is transferred to a single constituent or in a more complex way, it is distributed among the other constituents before the final-state pions emerge. Hence the target-proton response could depend only on the four-momentum and not on how it was transmitted.

For higher values of t and/or higher missing mass where no pion distributions for electroproduction presently exist, the pion distributions in the proton data change dramatically. Although we can still describe the x distribution by Ae^{-Bx} and the transverse momentum distribution by $Ae^{-Bp_{\perp}^2}$, all of the fit parameters except the transverse momentum slope change dramatically with t . There is some evidence²⁴ that this change in the pp data is associated with a shift in the dominant production mechanism from target excitation at low t to beam excitation at high t . This may be the onset of hadronic constituent scattering. In this regard, a comparison of the pp data presented here with ep or μp data at higher t and W when they become available could be illuminating.

*Work performed under the auspices of the Energy Research and Development Administration.

† Present address: Iowa State University, Ames, Iowa 50010.

‡ Present address: Singer-Kearfott Company, Wayne, New Jersey 07470.

§ Present address: Centre de Recherches Nucléaires, B.P. 20 CR, F67037 Strasbourg, France.

|| Present address: Fermi National Accelerator Laboratory, Batavia, Illinois 60510.

¶ Present address: CERN, 1211 Geneva 23, Switzerland.

¹T. T. Wu and C. N. Yang, Phys. Rev. **137**, 708 (1965).

²H. D. I. Abarbanel, S. D. Drell, and F. J. Gilman, Phys. Rev. **177**, 2458 (1969).

³S. M. Berman and M. Jacob, Phys. Rev. Lett. **25**, 1683 (1970).

⁴J. V. Allaby *et al.*, Phys. Lett. **33B**, 429 (1970).

⁵E. D. Bloom *et al.*, Phys. Rev. Lett. **23**, 930 (1969).

⁶A summary of recent experimental findings is provided by F. W. Brasse, in *Proceedings of the Sixth International Symposium on Electron and Photon Interactions at High Energies, Bonn, Germany, 1973*, edited by H. Rollnik and W. Pfeil (North-Holland, Amsterdam, 1974).

⁷For example see F. J. Gilman, lectures presented at the Summer Institute on Particle Interactions at Very High Energies, Louvain, Belgium, 1973 [SLAC Report

No. SLAC-PUB-1338 (unpublished)].

⁸For reaction (1) the cross section is only a function of q^2 and W ; however, for reaction (2) it can also be a function of energy.

⁹E. W. Anderson *et al.*, Nucl. Instrum. Methods. **122**, 587 (1974).

¹⁰J. R. Ficenece *et al.*, Nucl. Instrum. Methods **113**, 535 (1973).

¹¹D. R. Gilbert *et al.*, Nucl. Instrum. Methods **116**, 501 (1974).

¹² p_{\max} is determined by considering W to contain a nucleon and a pion: $W = (m_p^2 + p_{\max}^2)^{1/2} + (m_\pi^2 + p_{\max}^2)^{1/2}$.

¹³P. H. Garbincius *et al.*, Phys. Rev. Lett. **32**, 328 (1974).

¹⁴V. Eckardt *et al.*, DESY Report No. 74/5 (unpublished).

¹⁵J. Ballam *et al.*, Phys. Lett. **56B**, 193 (1975).

¹⁶A. Ramanaukas *et al.*, Phys. Rev. Lett. **31**, 1371 (1973).

¹⁷As is done in electroproduction, we fold the ϕ distribution at $\phi=0$.

¹⁸I. Dammann *et al.*, Nucl. Phys. **B54**, 381 (1973).

¹⁹C. J. Bebek *et al.*, Nucl. Phys. **B75**, 20 (1974).

²⁰J. T. Dakin *et al.*, Phys. Rev. D **10**, 1401 (1974).

²¹V. Eckardt *et al.*, Nucl. Phys. **B55**, 45 (1973).

²²L. Ahrens *et al.*, Phys. Rev. D **9**, 1894 (1974).

²³See for example E. L. Berger, in Proceedings of Ecole d'Eté de Physique des Particules, Gif sur Yvette, France, 1973 (unpublished).

²⁴L. J. Gutay *et al.* (unpublished).